# *Neisseria gonorrhoeae* FitA Interacts with FitB To Bind DNA through Its Ribbon−Helix−Helix Motif†

J. Scott Wilbur,*,‡ Peter T. Chivers,§ Kirsten Mattison,|| Laura Potter,‡ Richard G. Brennan,|| and Magdalene So‡

*Department of Molecular Microbiology and Immunology, and Department of Biochemistry, School of Medicine, Oregon Health and Sciences University, 3181 SE Sam Jackson Park Road, Portland, Oregon 97239, and Department of Biochemistry and Molecular Biophysics, Washington University School of Medicine, St. Louis, Missouri 63110*

*Received June 9, 2005; Revised Manuscript Received July 12, 2005*

ABSTRACT: The *fit* locus, encoding two proteins, FitA and FitB, was identified in a genetic screen for *Neisseria gonorrhoeae* determinants that affect trafficking across polarized epithelial cells. To better understand how the locus may control these activities, we have undertaken a biochemical analysis of FitA and FitB. FitA is a DNA-binding protein with a putative ribbon−helix−helix (RHH) motif. Purified FitA forms a homodimer that binds a 150 bp *fit* promoter sequence containing the translational start site. A putative $\beta$ strand mutant of FitA, FitA(R7A), is unable to bind this DNA, supporting further that FitA is a RHH protein. FitB interacts with FitA to form a 98 kDa complex. FitA/B binds DNA with a 38-fold higher affinity than the FitA homodimer. In DNase I footprint assays, FitA/B protects a 62-bp region within the *fit* promoter containing the predicted −10 sequence and an 8-bp inverted repeat, TGCTATCA-$N_{12}$-TGATAGCA. FitA/$B_{His}$ is able to bind to either half-site alone with high affinity.

*Neisseria gonorrhoeae* (GC,[1] gonococcus) is a sexually transmitted pathogen that infects only man. Infection is usually initiated at the mucosal epithelium of the urogenital tract (*1*). Because of its specificity for a number of human proteins (*2*−*7*) interactions between GC and host tissues have been studied mainly using human cell culture systems (*8*−*12*). These studies have shed light on the molecular and cell biology of GC attachment, cell entry, and intracellular survival (*13*−*17*). In contrast, the mechanisms used by GC to cross the epithelial barrier are not well understood. Studies on transcellular trafficking using monolayers of polarized T84 human colorectal carcinoma cells have shown that piliated GC not expressing Opa (a protein that influences attachment and invasion; *18*) cross the epithelial barrier in 24−36 h after inoculation onto the apical membrane (*9*). In contrast, *Neisseria meningitidis*, a closely related pathogen with very similar virulence factors, crosses this monolayer within 6 h.

We identified a chromosomal locus in GC that plays a role in transcellular trafficking and intracellular growth called *fit* (*f*ast *i*ntracellular *t*rafficking; *9*, *14*, *19*). Mutants with transposon insertions in *fit* cross polarized T84 monolayers five to six times more quickly than their wild-type (wt) parent strain. Moreover, *fit* mutants are altered in their intracellular behavior: they replicate within epithelial cells more quickly than the wt parent, though their replication in liquid medium is unaffected.

The *fit* locus encodes two open reading frames (ORF), *fitA* and *fitB*. The ORFs are tandemly arranged with a +1 base overlap; i.e., the last base of the *fitA* stop codon serves as the first base of the *fitB* start codon. FitA has a predicted molecular mass of 8.4 kDa and a p*I* of 6.6. FitB is predicted to be a 15.3 kDa protein with a p*I* of 5.8. Neither FitA nor FitB has a Sec signal sequence. Preliminary analysis suggested that the products of the *fit* locus are cytosolic and that FitA may interact with DNA (*19*).

Detailed biochemical knowledge of the *fit* proteins is crucial for understanding the role of the locus in gonococcal pathogenesis. We had hypothesized that FitA binds DNA and, through this interaction, regulates bacterial division and trafficking within the host cell. Here we report that FitA binds to its own promoter through a putative ribbon−helix−helix motif (RHH). RHH motifs have been identified and studied in numerous proteins with DNA-binding activity (*20*−*24*). This motif consists of a $\beta$ strand followed by two $\alpha$ helices (*25*). The $\beta$ strand inserts into the major groove of the DNA and is involved in sequence recognition (*21*, *26*). The two $\alpha$ helices are primarily involved in dimer formation. Many members of this family of proteins are autoregulatory. Arc, NikR, CopG, and Mnt bind as homotetramers to sequences within their own promoters (*21*, *26*−*29*). The binding sites of these proteins consist of two 6−8-bp half-sites, separated by 1−16 bp of intervening sequence.

Our studies revealed that FitB forms a complex with FitA and this complex increases the DNA-binding affinity of FitA. All other RHH proteins bind DNA without the help of a second protein, although the MetJ and NikR repressors require small molecule activators for DNA binding (*S*-

† This work was funded by NIH Grant 5RO1 AI47260-05.

* To whom correspondence should be addressed. E-mail: wilburj@ohsu.edu. Phone: 503-494-6840. Fax: 503-494-6862.

‡ Department of Molecular Microbiology and Immunology, Oregon Health and Sciences University.

§ Department of Biochemistry and Molecular Biophysics, Washington University School of Medicine.

|| Department of Biochemistry, School of Medicine, Oregon Health and Sciences University.

[1] Abbreviations: GC, *Neisseria gonorrhoeae*, gonococcus; ORF, open reading frame; RHH, ribbon−helix−helix motif; FitIS, Fit interaction sequence; FitPP, Fit perfect palindrome.

10.1021/bi0511080 CCC: $30.25 
Published on Web 08/19/2005

adenosylmethionine and nickel, respectively; *30*, *31*), and ParG is negatively affected in its DNA-binding activity upon complexing with ParF (*32*). Thus, FitA appears to be a novel member of the RHH family of proteins, the DNA-binding activity of which is positively affected by FitB.

## EXPERIMENTAL PROCEDURES

*Preparation of DNA.* PCR assays were performed using Pfu polymerase (Stratagene). The template for PCR amplifications was chromosomal DNA from the *Neisseria gonorrhoeae* strain FA1090 and was purified as described (*19*). PCR was performed for 30 cycles: 30 s at 96 °C, 30 s at 50 °C, and 60 s at 72 °C, unless otherwise indicated. DNA for gel retardation assays was prepared by PCR amplification, end-labeled with [α-$^{32}$P]ATP using T4 kinase (Invitrogen), and purified on ProbQuant G-50 microcolumns (Amersham Biosciences) as per manufacturer's instructions. Oligonucleotide pairs for fragments were as follows: $fit_{pro}$, Stbpre402 and StbL108; fragment 1, StbL108 and JSWanti-64; fragment 2, StbL108 and JSWanti-65; fragment 3, JSW64 and Stbpre402; fragment 4, JSW65 and Stbpre402; fragment 5, JSW64 and JSWanti-65. PCR annealing temperature for fragments 1−5 was 45 °C.

$JSW_{220}$ was generated by PCR amplification using the oligonucleotide primers JSW65 and StbR205. The amplified fragment was then cloned into the vector pCR-Blunt II (Invitrogen). DNA fragments were excised from this vector by restriction digest, and the single-stranded 3′ overhang of one of the sites was filled with Klenow fragment (Roche) and [γ- $^{32}$P]dATP (Invitrogen) in restriction digest buffer. "Plus" strand labeled DNA was generated by cutting with *Hin*dIII (filled) and then *Eco*RV in buffer B (Roche). "Minus" strand labeled DNA was generated by cutting with *Xba*I (filled) and then *Spe*I in buffer H (Roche). Labeled DNA fragments were purified on a 6% TBE (90 mM Tris−borate, 2 mM EDTA) polyacrylamide gel and resuspended in $H_2O$.

*Overexpression and Purification of Histidine Fusion Proteins.* The *fitA* ORF was amplified by PCR using the oligonucleotides PETFit5′.*Nco*I and FitA.*Xho*I-3′. PCR was performed as described above. These primers amplify a DNA fragment that begins at the *fitA* start codon and ends at its last codon, just prior to the stop codon; it also includes the restriction sites *Nco*I and *Xho*I at each end of the ORF to facilitate cloning. The *fitA* insert, excised with *Nco*I and *Xho*I, was ligated into the appropriately digested vector pET28b (Invitrogen) for overexpression. This vector added a T7 promoter and sequences encoding six histidine residues to the 5′ terminus of the *fitA* ORF. The resulting plasmid (pET28b::*fitA*) was transformed into the *Escherichia coli* strain BL21 (pLysE, Invitrogen) for overexpression. This protocol was also used to construct vectors for overexpression of $FitA/B_{His}$ (pET28b::$fitA/B_{His}$) and $FitA(R7A)_{His}$ [pET28b::$fitA(R7A)_{His}$]. Oligonucleotides used for construction of $fitA/B_{His}$ were PETFit5′.*Nco*I and PETFit3′.*Xho*I. Oligonucleotides for construction of $fitA(R7A)_{His}$ were FitA.R7A.*Nco*I and FitA.*Xho*I-3′. This last pair of oligonucleotides contains an alanine codon at the seventh position instead of arginine. $FitA(R7A)/B_{His}$ (pET28b::$fitR7A/B_{His}$) was constructed using the oligonucleotides FitA.R7A.*Nco*I and PETFit3′.*Xhi*I. All constructs were confirmed by sequencing analysis.

Protein overexpression and purification were performed as follows. Fourteen hour Luria broth (LB) cultures of each strain were diluted 1:100 in the same medium supplemented with kanamycin (60 μg/mL) and incubated for 2 h at 37 °C. Protein expression was induced by the addition of IPTG (0.5 mM) and further incubation at 37 °C for 2 h. Bacteria were then collected by centrifugation, and the pellets were resuspended and lysed in Bugbuster protein extraction reagent with benzonase (Novagen) per manufacturer's instruction. Protein was then purified using a His bind kit (Novagen) per manufacturer's instructions. Briefly, bacterial lysates were loaded onto a 10 mL column from the His bind kit, and the column was washed with 10 column volumes of binding buffer (5 mM imidazole, 0.5 M NaCl, 20 mM Tris-HCl, pH 7.9) and then 6 column volumes of wash buffer (60 mM imidazole, 0.5 M NaCl, 20 mM Tris-HCl, pH 7.9). The His-tagged protein was eluted with 5 mL of elution buffer (1 M imidazole, 0.5 M NaCl, 20 mM Tris-HCl, pH 7.9) and then concentrated with a 10 kDa Centricon centrifugal filter device (Amicon). $FitA/B_{His}$ was eluted from the nickel column in the elution buffer described above with the addition of 10 mM $MgCl_2$. Protein concentration was determined with a protein assay (Bio-Rad), using BSA as a standard.

*Gel Retardation Assays.* Binding reactions were performed according to published protocol (*33*). Briefly, binding was determined by incubating purified His-tagged protein with radiolabeled DNA in binding buffer [0.1 mM poly(dIdC), 25 mM Tris-HCl, 10 mM $MgCl_2$, 50 mM NaCl, pH 7.5] in a total volume of 20 μL at 37 °C for 30 min. Samples were then incubated at 4 °C for 10 min, and the products were separated in a native 4% polyacrylamide gel (80:1 acrylamide:bisacrylamide, 12 mM Tris−acetate, pH 7.5, 1 mM EDTA), 25−30 V at 4 °C for 8−10 h. Note: Samples were loaded onto the gels with the current running so bands at one end will be slightly higher than those at the other end. To compensate for this, we loaded no protein control at each end of the gel. Gels were then anchored to 3MM Whatman paper, covered in plastic wrap, and exposed to film (X-Omat Blue XB1, Kodak) at −80 °C.

*DNase I Footprinting Assays.* Binding reactions (20 μL) were prepared as above. Samples were incubated at 37 °C for 30 min and then with 1 μL of DNase I (0.01 unit/μL; Roche) at 25 °C for 2 min (*33*). Reaction mixtures were terminated by adding 1 μL of 0.5 M EDTA and incubated at 4 °C for 10 min. DNA fragments were then precipitated with ethanol (75%), sodium acetate (90 mM), and glycogen (1%) and frozen for >14 h at −80 °C. Pellets were collected by centrifugation, then resuspended in stop buffer (95% formamide, 20 mM EDTA, 0.05% bromophenol blue, 0.05% xylene cyanol FF), and then incubated at 80 °C for 5 min. The reaction products were then separated by electrophoresis on a sequencing gel (6% 30:1 acrylamide, 6 M urea, TBE buffer), and the radioactive bands were detected by autoradiography (X-Omat AR, Kodak) at −80 °C.

*Secondary Structure and Thermal Stability.* Circular dichroism experiments were performed on a Jasco J715 spectropolarimeter in 20 mM phosphate buffer (pH 7.5) using a 1 cm path length cuvette. Far-UV CD spectra were collected in triplicate from 260 to 200 nm (0.5 nm step size, 4 s averaging time). Thermal denaturation curves were

Table 1: Oligonucleotide Primers Used for Construction of Probes for Gel Retardation and Footprint Assays and Fluorescence Anisotropy[a]

| | |
|---|---|
| PETFit.*Nco*I | CCATGGCTTCTGTTGTGATTAG |
| FitA.*Xho*I-3′ | CTCGAGCAAAGAAACCTCGTTATCAG |
| PETFit3′.*Xho*I | CTCGAGGTGCCACGGATTGAACACCG |
| FitA.R7A.*Nco*I | CCATGGCTTCTGTTGTGATCGCGAATTTATCC |
| Stbpre402 | TGCCTTTCCTTCCTGAAAAAAGTTTTTC |
| StbL108 | TACCGAATCGGAAGCGGCAC |
| JSW65 | ATTTATCAGAAAGCGGGAGGGGAGACG |
| JSWanti-65 | CGTCTCCCCTCCCTCTTTCTG |
| JSW64 | ACAGAATTCAGTCCCTGAAAGCCGC |
| JSWanti-64 | GCGGCTTTCAGGGACTGAATTCTG |
| StbR205 | GCACGGAATTTGATTGCGTTG |
| IR36 fwd | F-AGATTGCTATCATTTTTTTTATTTTGATAGCATTTG |
| IR36 rev | CAAATGCTATCAAAATAAAAAAAAATGATAGCAATCT |
| IR36-1 fwd | F-AGATATACTGTCTTTTTTTTATTTTGATAGCATTTG |
| IR36-1 rev | CAAATGCTATCAAAATAAAAAAAAACTATCGTATCT |
| IR36-2 fwd | F-AGATTGCTATCATTTTTTTTATTTGACAGTATTTTG |
| IR36-2 rev | CAAAACTATCGTAAATAAAAAAAATGATAGCAATCT |
| IR36-3 fwd | F-AGATATACTGTCTTTTTTTTATTTGACAGTATTTTG |
| IR36-3 rev | CAAAATACTGTCAAATAAAAAAAAGACAGTATATCT |
| IR36-4 fwd | F-AGATTGCTATCAGGGGGGGGGGGGTGATAGCATTTG |
| IR36-4 rev | CAAATGCTATCACCCCCCCCCCCCTGATAGCAATCT |
| IR36-5 fwd | F-TAGATTGCTATCATTTTTTATTTTGATAGCATTTGT |
| IR36-5 rev | ACAAATGCTATCAAAATAAAAAATGATAGCAATCTA |
| IR36-6 fwd | F-TTTAGATTGCTATCATTATTTTGATAGCATTTGTTT |
| IR36-6 rev | AAACAAATGCTATCAAAATAATGATAGCAATCTAAA |
| IR36-7 fwd | F-TTTTTAGATTGCTATCATTTGATAGCATTTGTTTAT |
| IR36-7 rev | AATAACAAATGCTATCAAATGATAGCAATCTTTTTT |
| FitIS16 fwd | F-AGATTGCTATCATTTT |
| FitIS16 rev | AAAATGATAGCAATCT |
| FitPP16 A/T fwd | F-AGATTGATATCATTTT |
| FitPP16 A/T rev | AAAATGATATCAATCT |
| FitPP16 G/C fwd | F-AGATTGCTAGCATTTT |
| FitPP16 G/C rev | AAAATGCTAGCAATCT |

[a] All oligonucleotides are listed 5′ to 3′. F- = 5′-fluorescein tag.

measured at 222 nm (1 °C step size, 16 s averaging time) using a NESLAB RTE111 water bath.

*Oligomeric State.* Sedimentation equilibrium experiments were performed with a Beckman XL-A analytical ultracentrifuge. FitA protein samples (10−100 $\mu$M) were in 20 mM Tris-HCl (pH 8.0) and 100 mM NaCl. FitA/$B_{His}$ samples (50−100 $\mu$M) were in 100 mM sodium phosphate (pH 8.0), 100 mM sodium chloride, and 100 mM imidazole, with or without 10 mM $MgCl_2$. Equilibrium experiments were carried out at 13000, 19000, and 24000 rpm for FitA and 11000, 18000, and 25000 rpm for FitA/$B_{His}$. Equilibrium was reached by 12 h at each speed for all samples. Data were fit to a single oligomeric species model using SCIENTIST. The calculated molecular masses of FitA (18997 Da) and FitA/$B_{His}$ (24787 Da) were determined using the amino acid sequence plus the sequence LEHHHHHH, which was introduced in the construction of $FitA_{His}$ and FitA/$B_{His}$. The partial molar volumes of $FitA_{His}$ (0.7315 mg/mL), FitA/$B_{His}$ (0.7444 mg/mL), and buffer densities (1.007 g/mL, $FitA_{His}$; 1.018 g/mL, FitA/$B_{His}$) were calculated using the program SEDNTERP.

The molecular mass of the FitA/$B_{His}$ complex was also determined by dynamic light scattering on a DynaPro molecular size instrument (Protein Solutions). Protein was concentrated to 7 mg/mL (~70 $\mu$M), filtered, and analyzed in a 10 mm cuvette. The data were then analyzed with a filter for bimodal distribution.

*Fluorescence Anisotropy/Polarization.* Fluorescence polarization (FP) was performed on a Beacon 2000 (Panvera, Invitrogen). All experiments were done with 5′-fluorescein-labeled DNA fragments, and millipolarization (mP) and millianisotropy (mA) values were monitored in response to increases in protein concentration. Oligonucleotide pairs are listed in Table 1. Each pair of complementary fragments was suspended in $H_2O$ at a 5 $\mu$M concentration, annealed following incubation at 100 °C for 20 min, and slowly cooled to ambient temperature (~23 °C) over a period of 60 min. All experiments were done in Fit binding buffer (25 mM Tris-HCl, pH 7.5, 10 mM $MgCl_2$ 50 mM NaCl).

FP experiments were done as previously described (*34*). The baseline was determined for 5 nM fluorescein-labeled DNA followed by addition of up to 3000 nM protein. Dissociation constants ($K_d$) were calculated using the equation $P = \{((P_{bound} - P_{free})[protein])/(K_d + [protein])\} + P_{free}$, where $P$ is the polarization measured at a given total protein concentration, $P_{free}$ is the initial polarization of free fluorescein-labeled DNA, and $P_{bound}$ is the maximum polarization of specifically bound DNA. The resulting binding curve was plotted using KaleidaGraph 3.5.

## RESULTS

*FitA Binds DNA as a Homodimer through a Ribbon−Helix−Helix (RHH) Motif.* Sequence profiling (*28*) of published bacterial protein sequences uncovered a potential RHH motif in FitA located between residues 1 and 45 (Figure 1A). RHH motifs consist of a $\beta$ strand that is involved in DNA sequence recognition, followed by two α helices that function in dimer formation. The putative FitA RHH domain contains these motifs: the Chou−Fasman algorithm predicted a $\beta$ strand between residues 1 and 11, and an α-helical region between residues 15 and 39, centered by a turn (Figure 1B).

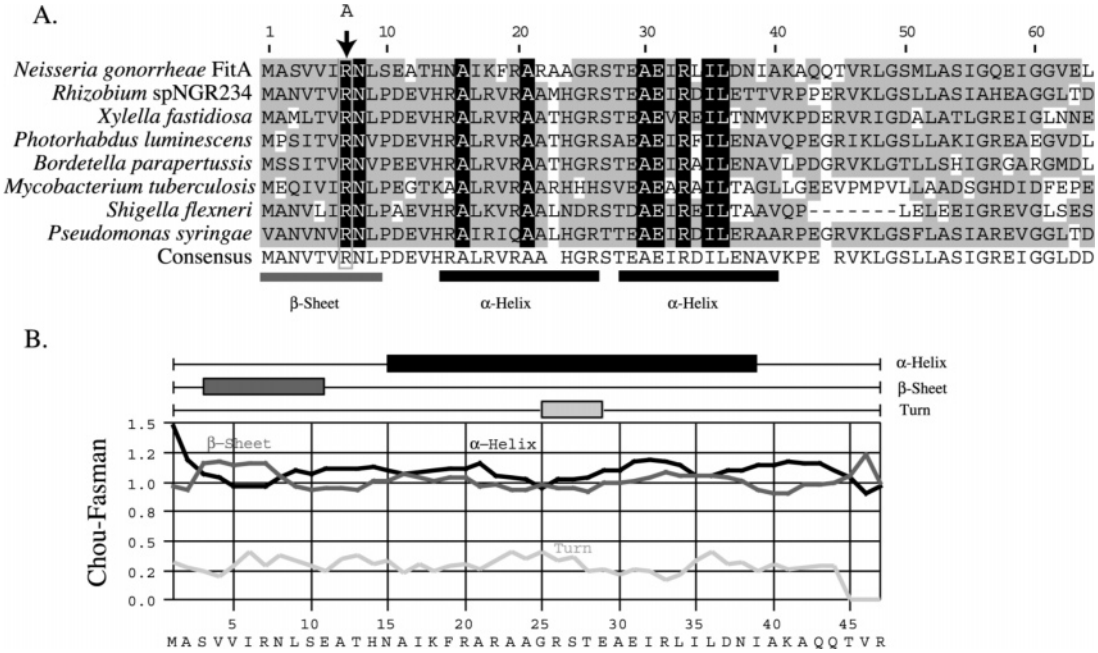


FIGURE 1: Bioinformatics analysis of FitA. (A) Clustal W alignment of the first 65 amino acids of FitA with homologues deduced from the genome sequences of other bacteria. Note that these homologues are hypothetical proteins. Homology is markedly reduced in the regions not pictured here. Key: White text on black boxes, residues with 100% sequence similarity; black text on gray boxes, highly conserved residues; black text on white boxes, nonconserved residues. Conserved arginine at position 7 is denoted by an arrow. (B) Chou−Fasman secondary structure prediction of the first 45 amino acids of FitA (the α-helix region is denoted by the black box above, the $\beta$ sheet region is denoted by the dark gray box, and the turn region is denoted by the light gray box).

The primary function of an RHH domain is to confer sequence-specific DNA binding. Moreover, many RHH proteins are autoregulatory, binding to inverted repeats within their own promoters to control transcription. We therefore examined the ability of FitA to bind its own promoter. The C terminus of FitA was tagged with six histidine residues by cloning the *fitA* ORF downstream of the T7 promoter in pET28b (Invitrogen). $FitA_{His}$ was overexpressed in *E. coli* BL21 by IPTG induction and purified (Figure 2A) as described in Experimental Procedures. Sedimentation equilibrium experiments carried out on $FitA_{His}$ revealed that the protein has an apparent molecular mass of 18573 Da (Table 2) compared to the predicted value of 18997 Da for a dimer.

Table 2: Biophysical Data for $FitA_{His}$ and $FitA(R7A)_{His}$

| | $T_m$ | | | $M_w$ | |
|---|---|---|---|---|---|
| protein | 2 $\mu$M | 5 $\mu$M | 10 $\mu$M | aa | AUC |
| $FitA_{His}$ | 53.9 | 57.5 | 60.4 | 18997 | 18573 |
| $FitA(R7A)_{His}$ | 53.6 | 56.7 (4 $\mu$M) | nd | 18827 | 18255 |

Additionally, the thermal stability of $FitA_{His}$ was concentration dependent (Table 2), as would be expected with a transition from folded dimer to unfolded monomers. These data suggest that $FitA_{His}$ forms a homodimer in the absence of FitB, consistent with the obligate dimeric nature of the RHH fold.

$FitA_{His}$ was next examined for its DNA-binding activity using a gel retardation assay. Varying amounts of $FitA_{His}$ were incubated, in the presence of poly(dIdC), with a fixed amount of $^{32}$P-labeled $fit_{pro}$, a 320-bp DNA fragment encompassing the region immediately upstream of the *fit* ORF (Figure 2F). $FitA_{His}$ bound to $fit_{pro}$ at $\geq$2.2 $\mu$M concentration (Figure 2B). This is a weak affinity for specific binding.

Deletion analysis of the $fit_{pro}$ fragment was next performed to determine if $FitA_{His}$ recognized a specific region of $fit_{pro}$. $FitA_{His}$, at a 2.2 $\mu$M concentration, was assessed for its ability to bind five overlapping $^{32}$P-labeled fragments covering the $fit_{pro}$ region (Figure 2C,F). $FitA_{His}$ shifted the mobility of fragments 3 and 4 but not the other fragments. This localizes the binding site to a 150-bp region immediately upstream of the *fitA* ORF. Gel retardation assays were also done with the fragment $JSW_{220}$. This fragment contained the 150 bp of fragment 4 and extends an additional 68 bp into the *fitA* ORF (Figure 2F). $FitA_{His}$ bound $JSW_{220}$ with a $K_d$ of approximately 1.5 $\mu$M (Figure 2D).

We next determined whether the putative RHH motif influences the DNA-binding activity of FitA. Alanine substitutions in the likely $\beta$ strand within the RHH of Arc and NikR abrogate DNA-binding activity without affecting the DNA-binding domain fold or the ability of these proteins to dimerize (*28*, *35*). The Chou−Fasman algorithm predicts that FitA residues 1−11 form part of a $\beta$ strand (Figure 1B), and a comparison of the FitA homologues reveals that the arginine in residue 7 is absolutely conserved in this region (Figure 1A). This arginine was replaced with alanine by site-directed mutagenesis, and the C terminus was His-tagged as described in Experimental Procedures. $FitA(R7A)_{His}$ was overexpressed in *E. coli* BL21 and purified as described for wt $FitA_{His}$ (Figure 2A). The secondary structure, thermal stability, and oligomeric state of $FitA(R7A)_{His}$ were virtually identical to $FitA_{His}$ (Table 2, Figure 3), indicating that the arginine to alanine mutation did not destabilize the RHH domain.

The effect of the R7A mutation on DNA binding was investigated using a gel retardation assay. $FitA(R7A)_{His}$ did not bind $JSW_{220}$ at a concentration of 12.0 $\mu$M (Figure 2D), indicating that this mutation decreased the DNA-binding

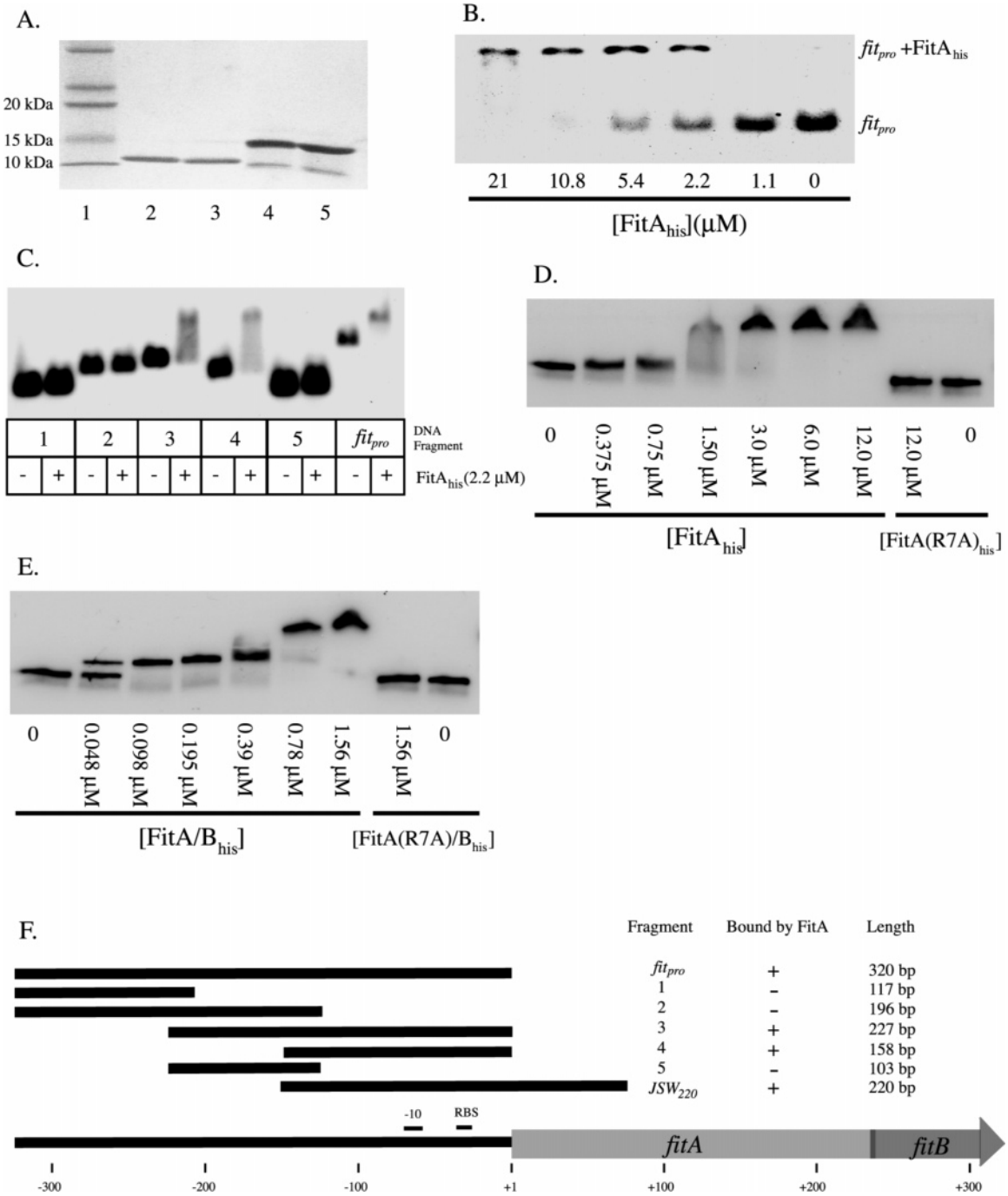


FIGURE 2: Analysis of the DNA-binding activity of $FitA_{His}$. (A) Purified His-tagged Fit proteins separated by SDS−PAGE and stained with Coomassie blue. Lanes: 1, molecular mass markers; 2, purified $FitA_{His}$; 3, $FitA(R7A)_{His}$; 4, $FitA/B_{His}$; 5, $FitA(R7A)/B_{His}$. N-Terminal sequencing (Edman degradation) was done on the protein added to lanes 4 and 5, revealing the proteins to be FitA [or FitA(R7A)] and FitB in a 1:1 ratio. (B) Gel retardation assay showing binding of varying amounts of $FitA_{His}$ to the $^{32}$P-labeled $fit_{pro}$ probe in the presence of poly(dIdC) (see diagram below). (C) Deletion analysis of the region of $fit_{pro}$ bound by 2.2 $\mu$M of $FitA_{His}$. (D) Gel retardation analysis of the binding affinity of $FitA_{His}$ and $FitA(R7A)_{His}$ to the $^{32}$P-labeled fragment $JSW_{220}$ in the presence of poly(dIdC). (E) Gel retardation analysis of the binding affinity of the $FitA/B_{His}$ and $FitA(R7A)/B_{His}$ complexes to the $^{32}$P-labeled fragment $JSW_{220}$ in the presence of poly(dIdC). Note: protein/DNA samples were added to the gel with current running. To compensate, we added no protein controls to each end of the gel. (F) Schematic of the *fit* locus and its upstream sequences (bottom diagram) and DNA fragments encoding segments of this region (fragments 1−5; $JSW_{220}$) used in gel retardation and footprinting assays.

affinity of the protein at least 8-fold. Additionally, $FitA(R7A)_{His}$ did not bind $fit_{pro}$ under any conditions tested (data not shown). Taken together, these results strongly suggest that FitA is a DNA-binding protein that makes specific contact with DNA through the RHH motif.

*FitB Forms a Complex with FitA.* FitB was His-tagged by cloning the *fitB* ORF downstream of the T7 promoter in pET28b, as described in Experimental Procedures. However, all attempts to overexpress soluble $FitB_{His}$ failed; the protein was partitioned into inclusion bodies (data not shown).

We next coexpressed *fitA* and *fitB* by cloning the *fitA/B* ORFs downstream of the T7 promoter in pET28b. This construction also placed a His tag at the C terminus of FitB. IPTG induction of this construct in *E. coli* BL21 yielded large amounts of soluble $FitB_{His}$ that could be recovered by nickel affinity column chromatography (Figure 2A). Fur-

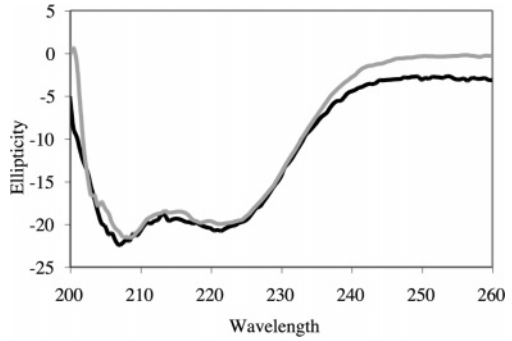


FIGURE 3: Circular dichroism analysis of $FitA_{His}$ (black) and $FitA(R7A)_{His}$ (gray).

thermore, fractions containing $FitB_{His}$ also contained an ~10 kDa protein. N-Terminal protein sequencing (Edman degradation) revealed the two proteins to be FitA and FitB in a 1:1 ratio. FitA therefore appears to increase the solubility of FitB. Fractions containing FitA and $FitB_{His}$ were examined further.

Dynamic light scattering (DLS) and analytical ultracentrifugation (AUC) were performed on the complex to determine its molecular mass. DLS was done on freshly purified protein, and the protein was found to be 95% monodisperse in a complex with a molecular mass of 98 kDa. AUC studies revealed the complex to sediment with an apparent molecular mass of 95 kDa. If the two proteins exist in a 1:1 ratio, the stoichiometry for the complex is likely to be $A_4B_4$, with a calculated molecular mass of 98247 Da. We therefore used a molecular mass of 98 kDa when calculating $FitA/B_{His}$ molarity.

*FitB Increases FitA DNA-Binding Affinity.* $FitA/B_{His}$ was next examined for its DNA-binding activity by gel retardation analysis. Increasing concentrations of the $FitA/B_{His}$ complex were incubated with $^{32}$P-labeled $fit_{pro}$ in the presence of poly(dIdC) and the products separated on a native gel. The $FitA/B_{His}$ complex began to bind $fit_{pro}$ at concentrations of ~0.190 $\mu$M (Figure 4A). $FitA/B_{His}$ formed two nucleoprotein complexes with $fit_{pro}$. The faster migrating complex was observed at a $FitA/B_{His}$ concentration of ~0.190 $\mu$M and the slower migrating complex at ≥0.765 $\mu$M (Figure 4A). The nature of these two complexes is unclear.

The $FitA/B_{His}$ binding site in the *fit* promoter region was also examined. $FitA/B_{His}$ (0.19 $\mu$M) was added to each of the five overlapping, PCR-generated, $^{32}$P-labeled fragments covering the $fit_{pro}$ region (see Figure 2F), and binding was assessed using the gel retardation assay. Like $FitA_{His}$ alone, $FitA/B_{His}$ bound only fragments 3 and 4 (Figure 4B).

We noted that $FitA/B_{His}$ has a higher affinity for binding to the $fit_{pro}$ fragment than FitA alone (2.2 $\mu$M $FitA_{His}$ vs 0.19 $\mu$M $FitA/B_{His}$). This was confirmed in additional binding assays using the $JSW_{220}$ fragment as probe. $FitA_{His}$ bound $JSW_{220}$ with a $K_d$ of ~1.50 $\mu$M. In contrast, $FitA/B_{His}$ bound $JSW_{220}$ with a $K_d$ of ~0.048 $\mu$M, indicating that the $FitA/B_{His}$ complex has a 20−30-fold higher affinity for this DNA than $FitA_{His}$ alone (Figure 2D,E).

When FitA(R7A) was coexpressed with $FitB_{His}$, both proteins could be recovered from the column (Figure 2A). The R7A mutation, therefore, does not affect the ability of FitA to interact with FitB. In addition, the $FitA(R7A)/FitB_{His}$ complex did not bind $JSW_{220}$ at a concentration of 1.56 $\mu$M (Figure 2E) or $fit_{pro}$ (data not shown). Compared to $FitA/B_{His}$, the affinity of the $FitA(R7A)/FitB_{His}$ mutant complex to DNA is decreased >30-fold. These experiments provide additional evidence that the DNA-binding activity of FitA is dependent on its RHH motif and that the FitA/B complex binds DNA primarily through this motif.

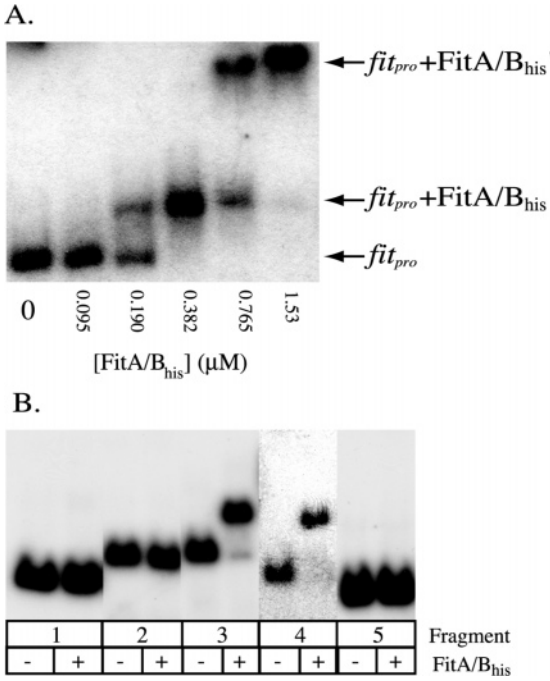


FIGURE 4: Gel retardation analysis of the DNA-binding activity of varying amounts of the $FitA/B_{His}$ complex with $^{32}$P-labeled $fit_{pro}$ (A) and $FitA/B_{His}$ with $^{32}$P-labeled fragments 1−5 at 1.53 $\mu$M (B).

*$FitA/B_{His}$ Binds DNA in a Sequence-Specific Manner.* DNase I footprinting analysis was employed to determine the sequences in the *fit* promoter region bound by $FitA/B_{His}$. $FitA/B_{His}$ bound both the plus and minus strands of fragment $JSW_{220}$ (Figure 5A,B). The complex protected the region between −60 and −17 bp in the minus strand and the region between −79 and −45 bp in the plus strand (Figure 5C). The protected region covers the putative −10 promoter sequence (TATCATT), though the transcriptional start site of FitA has not yet been mapped.

These $FitA/B_{His}$ binding studies also revealed DNase I hypersensitive sites in $JSW_{220}$, three on the minus strand at −24 (T), −41 (A) ,and −57 (G) and three on the plus strand at −47 (T), −55 (A), and −79 (G). Although these results suggest that the DNA bound by FitA/B undergoes a structural modification, further analysis will be required to determine how FitA/B causes this hypersensitivity.

Repeated attempts to obtain a footprint of $FitA_{His}$ bound to $JSW_{220}$ were unsuccessful. $FitA_{His}$ alone marginally protected $JSW_{220}$ from DNase I digestion, but we were unable to resolve a clear footprint. Failure of $FitA_{His}$ to footprint is likely due to the lower DNA-binding affinity of FitA in the absence of FitB, and this complex is not sufficiently stable to protect the DNA from cleavage by DNase I.

*$FitA_{His}$ and $FitA/B_{His}$ Bind the Sequence TGCTATCA.* The DNase I footprinting experiments localized binding of the $FitA/B_{His}$ complex to a 62-bp region of DNA. This fragment contains the inverted repeat TGCTATCA-$N_{12}$-TGATAGCA. A double-stranded DNA fragment corresponding to this inverted repeat with 4 bp of adjacent sequence was synthesized, termed IR36, fluorescein tagged on the 5′ end, and

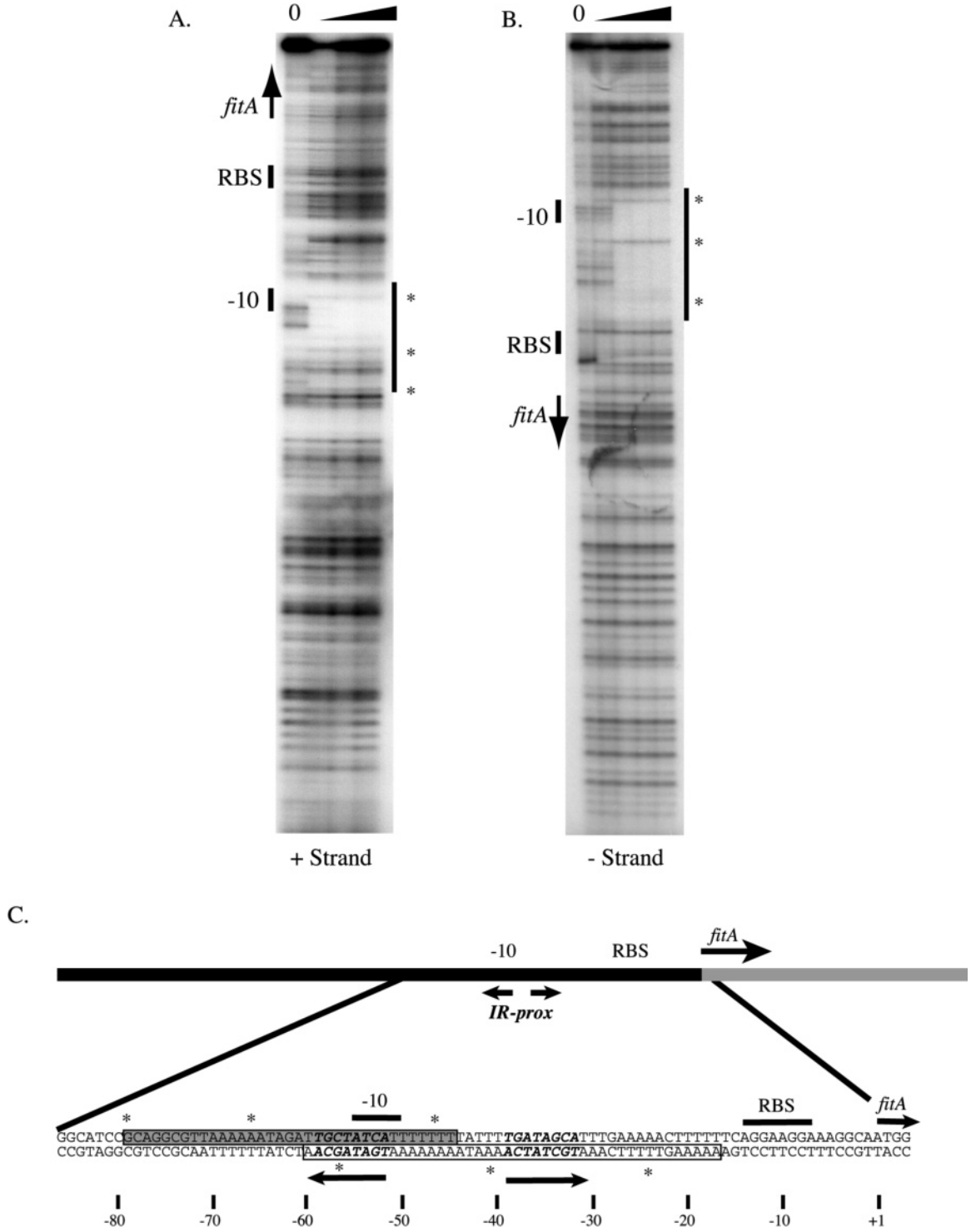


FIGURE 5: DNase I footprinting analysis of the FitA/$B_{His}$ complex to the plus (A) and minus (B) strand of *JSW*$_{220}$. Protein concentrations used were 0.675, 1.35, and 2.73 $\mu$M in (A) and 0.43, 0.675, 1.35, and 2.73 $\mu$M in (B). The region protected from DNase I digestion is indicated by the black line, and DNase I hypersensitive cleavage sites created by FitA/$B_{His}$ binding are shown with asterisks. (C) Diagram of *fit* promoter sequences protected by FitA/$B_{His}$ in the plus strand (gray box) and minus strand (open box). $IR_{prox}$ and divergent arrows indicate the inverted repeat at the putative −10 sequence.

analyzed by fluorescence anisotropy/polarization (FP) for its ability to bind $FitA_{His}$ and FitA/$B_{His}$ (Table 3). FitA/$B_{His}$ bound the IR36 fragment with a very high affinity ($K_d$ = 4.5 ± 0.7 nM); in comparison, $FitA_{His}$ bound this fragment with a $K_d$ of 178 ± 34 nM, a decrease of 38-fold. This enhancement of FitA DNA binding by FitB is consistent with our gel shift findings (Figure 6).

We hypothesized that $FitA_{His}$ and FitA/$B_{His}$ were binding to the inverted repeat sequence. To demonstrate this interaction, we analyzed the binding properties of oligodeoxynucleotides derived from IR36 with alterations in the inverted repeat sequence. $FitA_{His}$ and FitA/$B_{His}$ bound to fragments with either half-site scrambled (IR36-1 and IR36-2, Table 3) but not to the fragment with both half-sites scrambled

Table 3: Fluorescence Anisotropy with IR-prox and $FitA_{His}$ or $FitA/B_{His}$

| fragment name | sequence of top strand oligonucleotide[a] | $K_d(FitA_{His})$ (nM)[b,c] | $K_d(FitA/B_{His})$ (nM)[c] |
|---|---|---|---|
| IR36 | 5′-AGATTGCTATCATTTTTTTTATTTTGATAGCATTTG | 176 ± 34 | 4.5 ± 0.7 |
| IR36-1 | 5′-AGATatactgtcTTTTTTTTATTTTGATAGCATTTG | 155 ± 33 | 14.1 ± 2.9 |
| IR36-2 | 5′-AGATTGCTATCATTTTTTTTATTTgacagtatTTTG | 132 ± 25 | 12.4 ± 1.5 |
| IR36-3 | 5′-AGATatactgtcTTTTTTTTATTTgacagtatTTTG | >3000 | >3000 |
| IR36-4 | 5′-AGATTGCTATCAgggggggggggTGATAGCATTTG | nd | 3.5 ± 0.5 |
| IR36-5 | 5′-tAGATTGCTATCATTTTttATTTTGATAGCATTTGt | nd | 4.2 ± 0.8 |
| IR36-6 | 5′-tttAGATTGCTATCAttATTTTGATAGCATTTGttt | nd | 7.6 ± 1.2 |
| IR36-7 | 5′-tttttAGATTGCTATCAttTGATAGCATTTGtttat | nd | 3.0 ± 0.6 |
| FitIS16 | 5′-AGATTGCTATCATTTT | nd | 70.7 ± 11 |
| FitPP16-A/T | 5′-AGATTGaTATCATTTT | nd | 45.7 ± 2.3 |
| FitPP16-G/C | 5′-AGATTGCTAgCATTTT | nd | >500 |

[a] Top strand of double-stranded oligodeoxynucleotide DNA target listed (underline, inverted repeat; lower case, sequence changed from wild type). The 5′ end of the top strand was fluorescein tagged. [b] nd = not determined. [c] $K_d$ calculated from a hyperbolic curve fit algorithm (KaleidaGraph). The associated error is that of the mP value deviation from the curve.

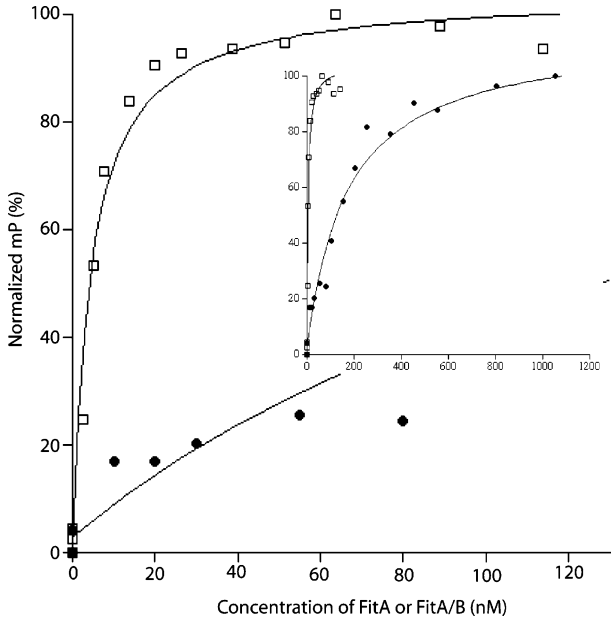


FIGURE 6: Binding isotherms of $FitA_{His}$ and $FitA/B_{His}$ to the IR36 DNA fragment. $FitA_{His}$ (●) bound this fragment with a $K_d$ of 176 nM, and $FitA/B_{His}$ (□) bound with a $K_d$ of 4.5 nM, a 38-fold higher affinity. These binding data were generated using the fluorescence anisotropy/polarization based DNA-binding assay, as described in Experimental Procedures. Note that FitA binding data above 150 nM are shown in the inserted graph.

(IR36-3). $FitA_{His}$ bound with equal affinity to the half-site mutants and to the wild-type fragment. $FitA/B_{His}$ bound these fragments with a 2.5-fold lower affinity, suggesting that, unlike $FitA_{His}$, the $FitA/B_{His}$ complex may be interacting with both half-sites.

We also examined the contribution of the 12-bp A/T-rich spacer region between the two half-sites to $FitA/B_{His}$ binding. This was done by either replacing the $(A/T)_{12}$ intervening sequence with $(G/C)_{12}$ (IR36-4) or changing the spacing and phase of the two half-sites with respect to each other. A 2-bp deletion brings the half-sites moderately out of phase (IR36-5). A 6-bp deletion orients the half-sites on opposite sides of the helix (IR36-6). Finally, a 10-bp deletion removes a whole turn, bringing the half-sites back into phase (IR36-7). $FitA/B_{His}$ bound to each of these four fragments with similar affinity (Table 3). These data suggest that FitA and FitA/B bind to the half-sites independently. To test this, DNA-binding assays were done on smaller oligodeoxynucleotides containing the 8-bp sequence TGCTATCA, which we termed *Fit i*nteraction *s*equence, FitIS (Table 3). $FitA/B_{His}$ did not bind to the 8-bp fragment alone, so longer fragments were analyzed. We found that $FitA/B_{His}$ bound a single half-site if the oligodeoxynucleotide length was 12 bp or greater (data not shown). $FitA/B_{His}$ bound a 16-bp fragment with an affinity of 70.7 ± 11 nM (FitIS16, Table 3). These data indicate that $FitA/B_{His}$ is able to bind the half-site independently, though with a diminished affinity.

The FitIS sequence is a pseudopalindrome, with 6 of its 8 bp forming an inverted repeat, TGCTATCA. Given the antiparallel arrangement of the $\beta$ strands involved in sequence recognition of RHH proteins (*21*, *23*), we thought FitA/B would bind a perfect palindrome better than the FitIS sequence. There are two possible perfect palindromes that can be made from FitIS with a single base pair change (FitPP16-A/T and FitPP16-G/C). $FitA/B_{His}$ bound the FitPP16-A/T fragment with an affinity of 45.7 ± 2.3 nM (1.5-fold better than FitIS16) but did not bind the FitPP16-G/C fragment.

Taken together, these data indicate that FitA and FitB form a complex with each other that binds the FitIS sequence TGCTATCA. The GC genome has 14 copies of FitID and four copies of TGATATCA, termed *Fit p*erfect *p*alindrome, FitPP (strain FA1090; http://www.stdgen.lanl.gov/). Two copies of FitIS form an inverted repeat in the *fit* promoter region. All other copies of the FitIS and FitPP occur as single copies. We have yet to determine if FitA/B binds to the other copies to the FitIS or FitPP and what consequence this binding may have in vivo.

## DISCUSSION

We have provided evidence that FitA binds its own promoter DNA and that the DNA recognition activity involves a ribbon−helix−helix motif. In the absence of FitB, FitA forms a homodimer in aqueous solution that binds specifically the DNA sequence TGCTATCA (FitIS) upstream of the *fitA* ORF. The affinity is relatively poor when compared with the binding affinities of other RHH proteins for their respective DNA-binding sites.

FitB interacts with FitA and increases its DNA-binding affinity. In turn, FitA greatly enhances the solubility of FitB. The FitA/B complex has a molecular mass of 98 kDa likely with a stoichiometry of $A_4B_4$. The FitA/B complex protects a 62-bp region of its promoter from DNase I digestion, and the complex binds the IR36 sequence within this region with a 38-fold higher affinity than the FitA homodimer. Moreover,

the interaction of FitA/B with DNA was dependent on the RHH domain of FitA as the R7A substitution abolishes DNA binding. FitA/B binds with a 2.5-fold higher affinity to DNA fragments containing two copies of FitIS than to fragments with a single copy. This difference in affinity was not observed with the FitA homodimer, indicating that the FitA/B complex is likely interacting with both of the FitIS half-sites. Additionally, we found that FitA/B was able to interact with palindromic sequence FitPP with higher affinity. These data suggest that FitA and FitA/B function as a regulator of its own transcription and, furthermore, that FitA(R7A) (the $\beta$-strand mutant) would not have this function. Studies are ongoing to demonstrate this activity.

The sequence TGCTATCA (FitIS) occurs 14 times in the GC genome, and the palindromic sequence TGATATCA (FitPP) occurs 4 times. Of these 18 potential binding sites, only 2 are located within promoter regions: those upstream of *fitA*. Of the rest, 12 are located within ORFs and 6 are found in predicted intergenic regions. These observations raise the question of whether FitA/B interacts with these sequences and, if so, whether such an interaction reflects a transcriptional regulatory function.

These studies demonstrate a novel interaction between a ribbon−helix−helix DNA-binding protein and a protein that positively affects its binding affinity. Crystallography studies are ongoing to determine the DNA-binding mechanism of FitA/B and to delineate the FitA−FitB interface that leads to high-affinity binding and heterooligomerization.

## ACKNOWLEDGMENT

We especially thank Sunghee Chai, Ken Haak, and Jay Mellies for advice and technical assistance in the preparation of the manuscript. We also thank Shaun Lee, Susan Clary, Nathan Weyand, and Eric Barklis for critical reading and ideas.

## REFERENCES

1. Handsfield, H., and Sparling, P. (1995) *Principles and Practice of Infectious Diseases*, Vol. 2, 4th ed., Churchill Liningstone, New York.
2. Cornelissen, C. N., Biswas, G. D., Tsai, J., Paruchuri, D. K., Thompson, S. A., and Sparling, P. F. (1992) Gonococcal transferrin-binding protein 1 is required for transferrin utilization and is homologous to TonB-dependent outer membrane receptors, *J. Bacteriol. 174*, 5788−5797.
3. Popp, A., Dehio, C., Grunert, F., Meyer, T. F., and Gray-Owen, S. D. (1999) Molecular analysis of neisserial Opa protein interactions with the CEA family of receptors: identification of determinants contributing to the differential specificities of binding, *Cell Microbiol. 1*, 169−181.
4. Chen, T., Grunert, F., Medina-Marino, A., and Gotschlich, E. C. (1997) Several carcinoembryonic antigens (CD66) serve as receptors for gonococcal opacity proteins, *J. Exp. Med. 185*, 1557−1564.
5. Kallstrom, H., Liszewski, M. K., Atkinson, J. P., and Jonsson, A. B. (1997) Membrane cofactor protein (MCP or CD46) is a cellular pilus receptor for pathogenic *Neisseria*, *Mol. Microbiol. 25*, 639−647.
6. Kallstrom, H., Blackmer Gill, D., Albiger, B., Liszewski, M. K., Atkinson, J. P., and Jonsson, A. B. (2001) Attachment of *Neisseria gonorrhoeae* to the cellular pilus receptor CD46: identification of domains important for bacterial adherence, *Cell Microbiol. 3*, 133−143.
7. Bonnah, R. A., Yu, R., and Schryvers, A. B. (1995) Biochemical analysis of lactoferrin receptors in the Neisseriaceae identification of a second bacterial lactoferrin receptor protein, *Microb. Pathog. 19*, 285−297.
8. McGee, Z. A., Johnson, A. P., and Taylor-Robinson, D. (1981) Pathogenic mechanisms of *Neisseria gonorrhoeae*: observations on damage to human Fallopian tubes in organ culture by gonococci of colony type 1 or type 4, *143*, 413−422.
9. Merz, A. J., Rifenbery, D. B., Arvidson, C. G., and So, M. (1996) Traversal of a polarized epithelium by pathogenic Neisseriae: facilitation by type IV pili and maintenance of epithelial barrier function, *Mol. Med. 2*, 745−754.
10. Merz, A. J., and So, M. (1997) Attachment of piliated, Opa- and Opc- gonococci and meningococci to epithelial cells elicits cortical actin rearrangements and clustering of tyrosine-phosphorylated proteins, *Infect. Immun. 65*, 4341−4349.
11. Harvey, H. A., Jennings, M. P., Campbell, C. A., Williams, R., and Apicella, M. A. (2001) Receptor-mediated endocytosis of *Neisseria gonorrhoeae* into primary human urethral epithelial cells: the role of the asialoglycoprotein receptor, *Mol. Microbiol. 42*, 659−672.
12. Harvey, H. A., Ketterer, M. R., Preston, A., Lubaroff, D., Williams, R., and Apicella, M. A. (1997) Ultrastructural analysis of primary human urethral epithelial cell cultures infected with *Neisseria gonorrhoeae*, *Infect. Immun. 65*, 2420−2427.
13. Meyer, T. F. (1999) Pathogenic neisseriae: complexity of pathogen-host cell interplay, *Clin. Infect. Dis. 28*, 433−441.
14. Merz, A. J., and So, M. (2000) Interactions of pathogenic neisseriae with epithelial cell membranes, *Annu. Rev. Cell Dev. Biol. 16*, 423−457.
15. Gray-Owen, S. D. (2003) Neisserial Opa proteins: impact on colonization, dissemination and immunity, *Scand. J. Infect. Dis. 35*, 614−618.
16. Lin, L., Ayala, P., Larson, J., Mulks, M., Fukuda, M., Carlsson, S. R., Enns, C., and So, M. (1997) The Neisseria type 2 IgA1 protease cleaves LAMP1 and promotes survival of bacteria within epithelial cells, *Mol. Microbiol. 24*, 1083−1094.
17. Ayala, P., Lin, L., Hopper, S., Fukuda, M., and So, M. (1998) Infection of epithelial cells by pathogenic neisseriae reduces the levels of multiple lysosomal constituents, *Infect. Immun. 66*, 5001−5007.
18. Wang, J., Gray-Owen, S. D., Knorre, A., Meyer, T. F., and Dehio, C. (1998) Opa binding to cellular CD66 receptors mediates the transcellular traversal of *Neisseria gonorrhoeae* across polarized T84 epithelial cell monolayers, *Mol. Microbiol. 30*, 657−671.
19. Hopper, S., Wilbur, J. S., Vasquez, B. L., Larson, J., Clary, S., Mehr, I. J., Seifert, H. S., and So, M. (2000) Isolation of *Neisseria gonorrhoeae* mutants that show enhanced trafficking across polarized T84 epithelial monolayers, *Infect. Immun. 68*, 896−905.
20. Raumann, B. E., Brown, B. M., and Sauer, R. T. (1994) Major groove recongnition by $\beta$-sheets: the ribbon-helix-helix family of gene regulatory proteins, *Curr. Opin. Struct. Biol. 4*, 36−43.
21. Raumann, B. E., Rould, M. A., Pabo, C. O., and Sauer, R. T. (1994) DNA recognition by beta-sheets in the Arc repressor-operator crystal structure, *Nature 367*, 754−757.
22. Sauer, R. T., Milla, M. E., Waldburger, C. D., Brown, B. M., and Schildbach, J. F. (1996) Sequence determinants of folding and stability for the P22 Arc repressor dimer, *FASEB J. 10*, 42−48.
23. Phillips, S. E. (1994) The beta-ribbon DNA recognition motif, *Annu. Rev. Biophys. Biomol. Struct 23*, 671−701.
24. Chivers, P. T., and Sauer, R. T. (2000) Regulation of high affinity nickel uptake in bacteria. $Ni^{2+}$-Dependent interaction of NikR with wild-type and mutant operator sites, *J. Biol. Chem. 275*, 19735−19741.
25. Somers, W. S., and Phillips, S. E. (1992) Crystal structure of the met repressor-operator complex at 2.8 Å resolution reveals DNA recognition by beta-strands, *Nature 359*, 387−393.
26. Gomis-Ruth, F. X., Sola, M., Acebo, P., Parraga, A., Guasch, A., Eritja, R., Gonzalez, A., Espinosa, M., del Solar, G., and Coll, M. (1998) The structure of plasmid-encoded transcriptional repressor CopG unliganded and bound to its operator, *EMBO J. 17*, 7404−7415.
27. Knight, K. L., and Sauer, R. T. (1992) Biochemical and genetic analysis of operator contacts made by residues within the beta-sheet DNA binding motif of Mnt repressor, *EMBO J. 11*, 215−223.
28. Chivers, P. T., and Sauer, R. T. (1999) NikR is a ribbon-helix-helix DNA-binding protein, *Protein Sci. 8*, 2494−2500.
29. Schreiter, E. R., Sintchak, M. D., Guo, Y., Chivers, P. T., Sauer, R. T., and Drennan, C. L. (2003) Crystal structure of the nickel-responsive transcription factor NikR, *Nat. Struct. Biol. 10*, 794−799.

30. Phillips, K., and Phillips, S. E. (1994) Electrostatic activation of *Escherichia coli* methionine repressor, *Structure 2*, 309−316.
31. Chivers, P. T., and Sauer, R. T. (2002) NikR repressor: high-affinity nickel binding to the C-terminal domain regulates binding to operator DNA, *Chem. Biol. 9*, 1141−1148.
32. Golovanov, A. P., Barilla, D., Golovanova, M., Hayes, F., and Lian, L. Y. (2003) ParG, a protein required for active partition of bacterial plasmids, has a dimeric ribbon-helix-helix structure, *Mol. Microbiol. 50*, 1141−1153.
33. Chai, S., and Alsonso, J. C. (1996) Distamycin-induced inhibition of formation of a nucleoprotein complex between the terminase small subunit G1P and the non-encapsidated end (pacL site) of *Bacillus subtilis* bacteriophage SPP1, *Nucleic Acids Res. 24*, 282−288.
34. Newberry, K. J., and Brennan, R. G. (2004) The structural mechanism for transcription activation by MerR family member multidrug transporter activation, N terminus, *J. Biol. Chem. 279*, 20356−20362.
35. Brown, B. M., Milla, M. E., Smith, T. L., and Sauer, R. T. (1994) Scanning mutagenesis of the Arc repressor as a functional probe of operator recognition, *Nat. Struct. Biol. 1*, 164−168.

BI0511080